Interleukin-27 inhibits ectopic lymphoid-like structure development in early inflammatory arthritis

Gareth W. Jones,[1] Michele Bombardieri,[3] Claire J. Greenhill,[1] Louise McLeod,[2] Alessandra Nerviani,[3] Vidalba Rocher-Ros,[3] Anna Cardus,[1] Anwen S. Williams,[1] Costantino Pitzalis,[3] Brendan J. Jenkins,[2]* and Simon A. Jones[1]*

[1]Division of Infection and Immunity, School of Medicine, Cardiff University, Cardiff CF10 3XQ, Wales, UK
[2]Centre for Innate Immunity and Infectious Diseases, Hudson (formerly Monash) Institute of Medical Research, Clayton, Victoria 3168, Australia
[3]Centre for Experimental Medicine and Rheumatology, William Harvey Research Institute, Barts and The London School of Medicine and Dentistry, Queen Mary University of London, John Vane Science Centre, London EC1M 6BQ, England, UK

Ectopic lymphoid-like structures (ELSs) reminiscent of secondary lymphoid organs often develop at sites of chronic inflammation where they contribute to immune-mediated pathology. Through evaluation of synovial tissues from rheumatoid arthritis (RA) patients, we now show that low interleukin-27 (IL-27) expression corresponds with an increased incidence of ELS and gene signatures associated with their development and activity. The presence of synovial ELS was also noted in mice deficient in the IL-27 receptor (IL-27R) after the onset of inflammatory arthritis. Here, pathology was associated with increased synovial expression of pro-inflammatory cytokines, homeostatic chemokines, and transcriptional regulators linked with lymphoid neogenesis. In both clinical and experimental RA, synovial ELS coincided with the heightened local expression of cytokines and transcription factors of the Th17 and T follicular helper (Tfh) cell lineages, and included podoplanin-expressing T cells within lymphoid aggregates. IL-27 inhibited the differentiation of podoplanin-expressing Th17 cells, and an increased number of these cells were observed in IL-27R–deficient mice with inflammatory arthritis. Thus, IL-27 appears to negatively regulate ELS development in RA through control of effector T cells. These studies open new opportunities for patient stratification and treatment.

CORRESPONDENCE
Simon A. Jones:
JonesSA@cf.ac.uk
OR
Gareth W. Jones:
JonesGW6@cf.ac.uk

Abbreviations used: ACP, anticyclic citrullinated peptide; ACPA, anticitrullinated protein/peptide antibodies; AIA, antigen-induced arthritis; CFA, complete Freund's adjuvant; ELISA, enzyme-linked immunosorbent assay; ELS, ectopic lymphoid-like structure; GC, germinal center; IF, immunofluorescence; IHC, immunohistochemistry; mBSA, methylated bovine serum albumin; OA, osteoarthritis; RA, rheumatoid arthritis; RF, rheumatoid factor; STAT3, signal transducer and activator of transcription 3.

Rheumatoid arthritis (RA) is characterized by an immune-mediated destruction of joint tissue caused by chronic inflammation of the synovium (Manzo et al., 2010). Synovitis in RA is highly heterogeneous and is classified according to specific histological features (Klimiuk et al., 1997; Pitzalis et al., 2013). In RA, synovial histopathology is defined as fibroblast- (or pauci immune), diffuse-, or lymphoid-rich. The latter is characterized as lymphoid follicle-like structures ranging from T and B cell aggregates to highly organized structures comprising follicular DC (fDC) networks reminiscent of germinal centers (GCs). These structures are present in ∼40% of RA patients (Manzo et al., 2010; Pitzalis et al., 2013) and are associated with severe disease, T cell priming, and autoantibody production (Takemura et al., 2001; Rosengren et al., 2008; Humby et al., 2009). Although circulating rheumatoid factor (RF) and anticitrullinated protein antibodies (ACPA) correlate with disease severity (Avouac et al., 2006), these clinical markers unreliably predict synovial pathology.

IL-27 is a regulator of adaptive immunity and limits T cell–driven pathology by restricting IL-2 activity and the expansion of IL-17–secreting T helper 17 (Th17) cells (Villarino et al., 2003; Owaki et al., 2006; Stumhofer et al., 2006). Recently, Th17 cells were shown to enhance ectopic lymphoid-like structure (ELS) formation in inflamed tissues (Peters et al., 2011; Rangel-Moreno et al., 2011). Indeed,

*B.J. Jenkins and S.A. Jones contributed equally to this paper.

The Rockefeller University Press $30.00
J. Exp. Med. 2015 Vol. 212 No. 11 1793–1802
www.jem.org/cgi/doi/10.1084/jem.20132307

The Journal of Experimental Medicine

Th17 cell plasticity permits the acquisition of Tfh-like effector characteristics that support ELS expansion and GC reactions (Lu et al., 2011; Peters et al., 2011; Hirota et al., 2013). In models of inflammatory arthritis, IL-27 blocks Th17-associated joint pathology (Niedbala et al., 2008; Pickens et al., 2011) and inhibits osteoclastogenesis to restrict bone erosion (Kalliolias et al., 2010). While elevated synovial and serum IL-27 levels have been observed in RA (Wong et al., 2010; Tanida et al., 2011), no study has considered the impact of IL-27 on synovial histopathology. Here, we show that IL-27 control of CD4 T cell responses prevents the development of synovial ELS.

RESULTS AND DISCUSSION

Synovial ELSs in RA contain IL-27R$^+$ lymphocytic aggregates

The IL-27 receptor comprises a heterodimeric complex of IL-27R (WSX-1) and gp130, the β-signaling receptor of the IL-6 cytokine family. To evaluate how IL-27R expression relates to local joint pathology, RA synovia were graded histologically for the presence or absence of ELS (Fig. 1 A and Fig. S1). Tissue with grade-3 (G3) ELS aggregates comprising CD3$^+$, CD20$^+$, and CD21$^+$ cells (ELS$^+$) were compared with biopsies displaying diffuse lymphocytic infiltrates (ELS$^-$). To validate our cellular characterization, expression of key homeostatic chemokines, cytokines, and molecular signatures of ELS were evaluated (Timmer et al., 2007; Humby et al., 2009). Consistent with the presence of lymphoid follicles, heightened *CXCL13*, *CCL19*, and *CXCR5* expression was observed in ELS$^+$ patient biopsies (Fig. 1 B). Elevated transcripts for activation-induced cytidine deaminase (AID), an enzyme involved in somatic hypermutation and class switching, was also observed (Fig. 1 B). Consistent with the presence of CD21$^+$ fDC networks detected by immunohistochemistry

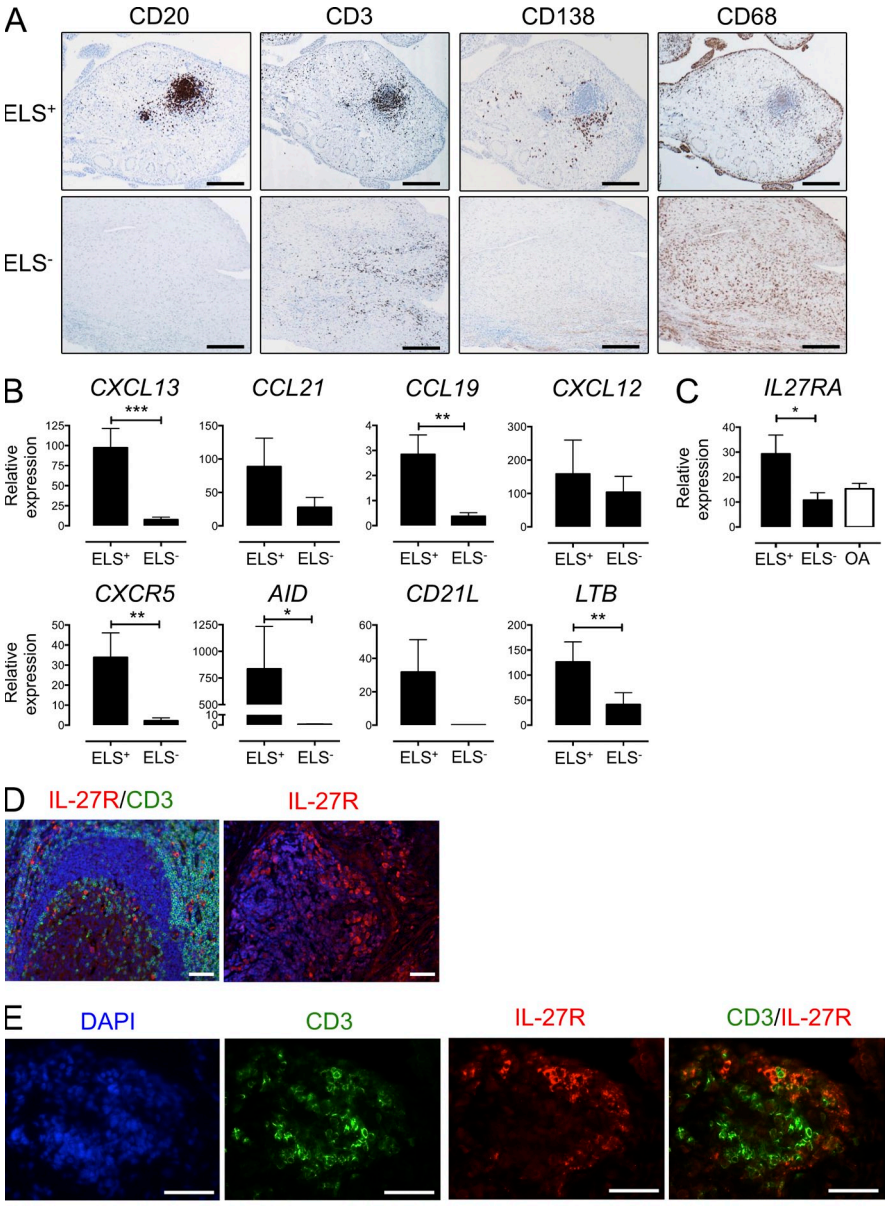

Figure 1. IL-27R is expressed at synovial ELS. (A) Representative histopathology of RA synovium from 59 patients with ELS (ELS$^+$) and diffuse pathology (ELS$^-$). Sequential sections were stained as indicated by IHC. (B) qPCR analysis of ELS$^+$ and ELS$^-$ synovia for the indicated genes (number of patients: *CXCL13* and *AID*, $n = 34$ ELS$^+$, $n = 24$ ELS$^-$; *CXCR5*, *CD21L*, and *LTB*, $n = 28$ ELS$^+$, $n = 20$ ELS$^-$; *CCL19* and *CCL21*, $n = 13$ ELS$^+$, $n = 12$ ELS$^-$; *CXCL12*, $n = 15$ ELS$^+$, $n = 8$ ELS$^-$). (C) *IL27RA* expression in ELS$^+$ and ELS$^-$ RA synovia. Synovial tissue from OA patients was used as control (error bars, SEM; $n = 19$ ELS$^+$, $n = 13$ ELS$^-$, $n = 11$ OA patients). (D) Detection of IL-27R in tonsil GCs (left) and synovial ELS (right) by IF for IL-27R and CD3, and DAPI counterstaining. Images are representative of three tissue samples. (E) IF for IL-27R and CD3 with DAPI nuclear staining in synovial ELS. Error bars indicate SEM. *, $P < 0.05$; **, $P < 0.01$; ***, $P < 0.001$. Bars: (A) 200 µm; (D and E) 50 µm.

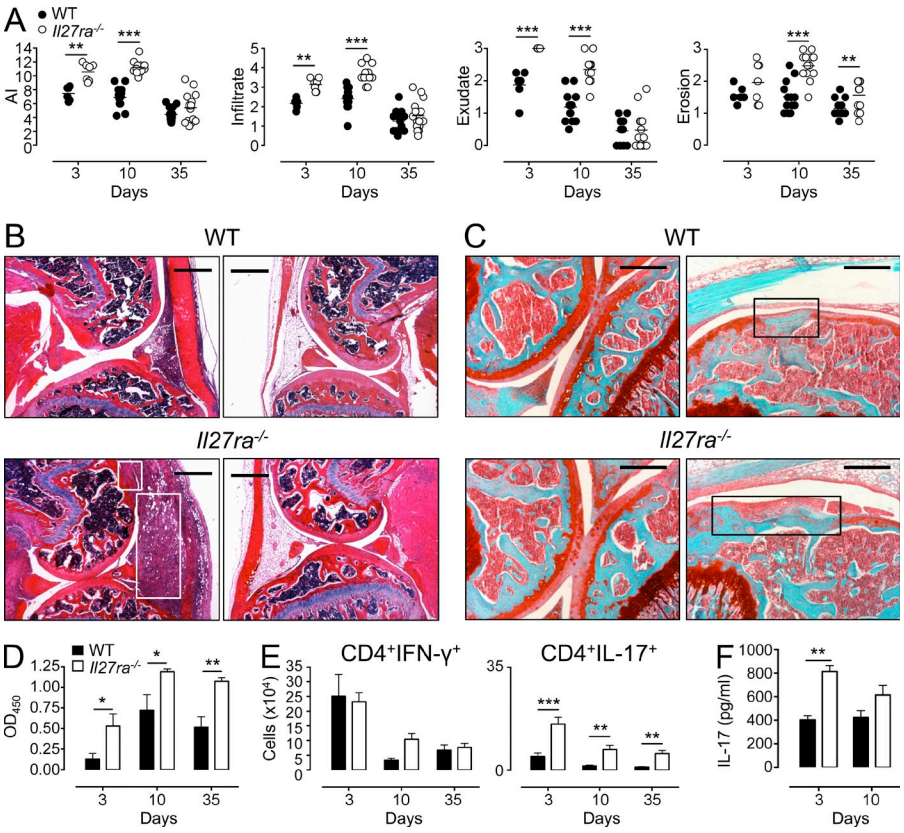

Figure 2. IL-27 is protective in inflammatory arthritis. (A) Histopathology scoring of AIA in WT and *Il27ra*$^{-/-}$ mice, showing arthritic index, synovial infiltration, exudate, and erosion at d3 (n = 6–7/group), d10 (n = 13/group), and d35 (n = 14–15/group). (B) Representative H&E of knee joints at d10 of AIA; boxed areas show extensive subsynovial inflammation (large box) and focal bone erosions (small box) in *Il27ra*$^{-/-}$ mice. Noninflamed control joints are shown on the right. (C) Representative images of cartilage degradation and bone erosion, seen as loss of red Safranin O staining of the articular cartilage. Boxes show focal bone erosions. (D) Anti-mBSA serum titers at d3 (n = 6–7/group), d10 (n = 5/group), and d35 (n = 6–8/group). (E) Number of IFN-γ– and IL-17–producing CD4 T cells in inguinal LNs determined by flow cytometry at d3 (n = 6–7/group), d10 (n = 8/group), and d35 (n = 14–15/group). (F) ELISA of serum IL-17 at d3 (n = 6–7/group) and d10 (n = 12–13/group) of AIA. Error bars indicate SEM. *, $P < 0.05$; **, $P < 0.01$; ***, $P < 0.001$. Data are presented from two independent experiments per time point. Bars: (B) 500 µm; (C) 300 µm.

(IHC), ELS$^+$ synovia showed expression of the long CD21 isoform (*CD21L*; Fig. 1 B). Heightened expression of lymphotoxin-β (LTB), a cytokine linked with lymphoid neogenesis, was also observed in ELS$^+$ synovia (Fig. 1 B). Interestingly, *IL27RA* expression was increased in ELS$^+$ patient synovia compared with ELS$^-$ and osteoarthritis (OA) control tissue (Fig. 1 C). Consistent with the pattern of IL-27R staining seen in tonsil tissue displaying highly organized GCs, immunofluorescence (IF) revealed IL-27R$^+$ cells within synovial ELS (Fig. 1 D). Here, IL-27R expression was largely observed in T cell–rich areas of lymphoid aggregates (Fig. 1 E). Thus, IL-27 may impact synovial ELS development or associated effector T cell activities.

IL-27R–deficient mice display severe inflammatory arthritis

To consider the impact of IL-27 on inflammatory arthritis, disease activity was monitored in WT and *Il27ra*$^{-/-}$ mice after the onset of antigen-induced arthritis (AIA; Nowell et al., 2009). *Il27ra*$^{-/-}$ mice displayed exacerbated joint pathology, as indicated by increases in leukocyte infiltration, synovial exudate, hypertrophy, and hallmarks of cartilage and bone erosion (Fig. 2, A–C). By day 35 (d35) of AIA, WT and *Il27ra*$^{-/-}$ mice displayed extensive cartilage degradation. However, an increased incidence of focal bone erosions was seen in *Il27ra*$^{-/-}$ mice (Fig. 2, A and C). These findings reveal a protective role for IL-27 in AIA and support the ability of IL-27 to inhibit RANKL-dependent and -independent osteoclastogenic bone erosion (Niedbala et al., 2008; Kalliolias et al., 2010; Pickens et al., 2011). Increased arthritis severity in *Il27ra*$^{-/-}$ mice was also linked with heightened adaptive immune responses. Specifically, *Il27ra*$^{-/-}$ mice showed elevated antigen (mBSA)-specific serum IgG titers (Fig. 2 D), increased Th17 cell numbers in draining LNs (Fig. 2 E), and a concomitant increase in serum IL-17 levels early after disease onset (Fig. 2 F).

Exacerbated synovitis in IL-27R deficiency is linked with ELS development

Based on IL-27 bioactivity and the pattern of IL-27R expression in human synovial biopsies, we next assessed the impact of IL-27R deficiency on the pattern of synovitis. *Il27ra*$^{-/-}$ mice with AIA showed heightened synovial T cell infiltration and the presence of discrete CD3$^+$ aggregates throughout the synovium (Fig. 3 A). Whereas a small proportion of mice presented with small aggregates at d3 after AIA (not depicted), by d10 all *Il27ra*$^{-/-}$ mice developed multiple lymphoid aggregates (7.1 ± 0.8 per synovial section and 12.8 × 10^4 ± 1.7 µm^2 in size; Fig. 3, A and B). WT mice developed a more diffuse pattern of synovial inflammation and showed significantly fewer lymphoid aggregates. When present, these were both smaller in size and less organized (1.9 ± 0.4 per synovial section and 1.6 × 10^4 ± 0.5 µm^2 in size; Fig. 3 B). Although the inflamed synovium of *Il27ra*$^{-/-}$ mice showed a paucity of B220$^+$ cells, IHC staining for B cells colocalized with the defined CD3$^+$-rich aggregates (Fig. 3 C). However, the degree of B cell involvement often varied between aggregates (e.g., compare Fig. 3 C and Fig. 5 A). Although

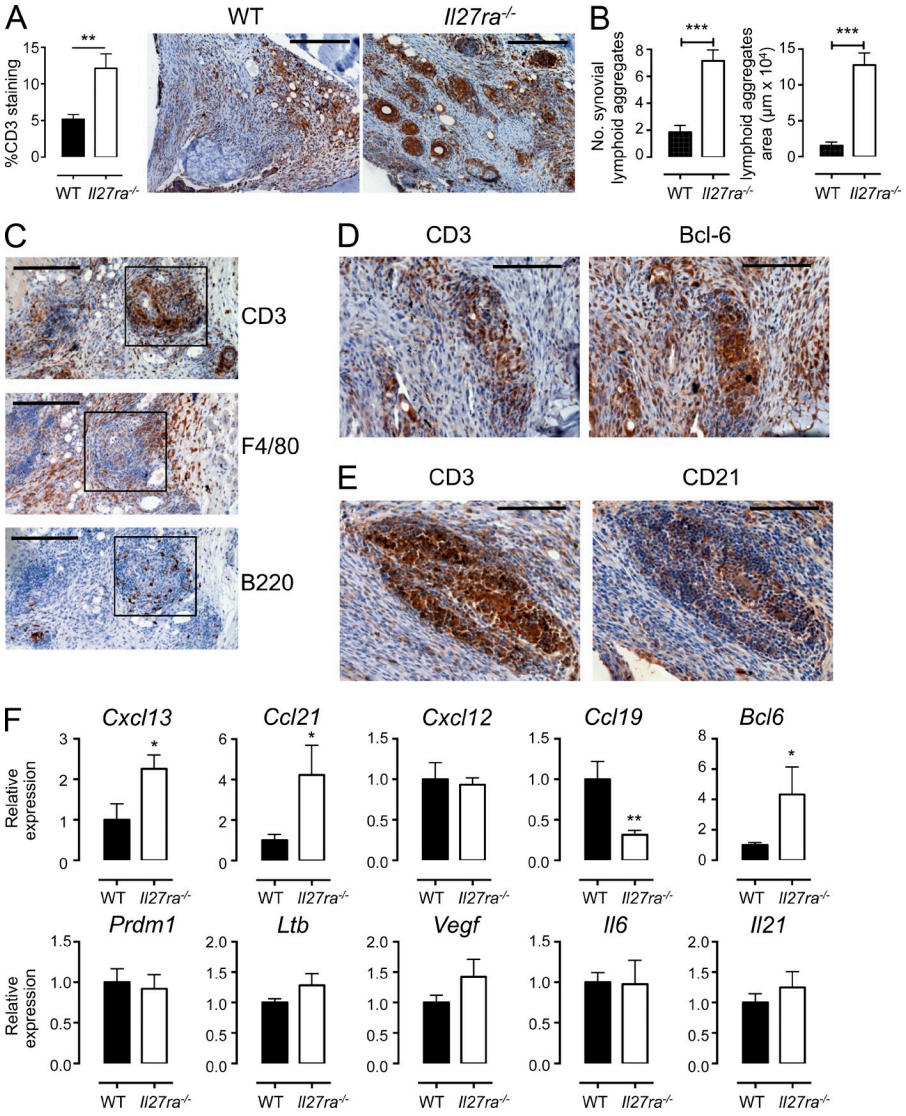

Figure 3. *Il27ra*$^{-/-}$ mice develop synovial ELS-like pathology. (A–F) AIA was established in WT and *Il27ra*$^{-/-}$ mice and histopathology assessed at d10. (A) Representative IHC and quantification of CD3 staining in synovial sections (n = 11–13/group). (B) The number (left) and area (right) of lymphoid aggregates were quantified in para-sagital synovial sections (n = 27–29/group). (C) Serial sections from *Il27ra*$^{-/-}$ mice were stained for CD3, F4/80, and B220. Aggregates in sequential sections are shown boxed. (D and E) Serial sections from *Il27ra*$^{-/-}$ mice stained for CD3 and Bcl-6 (D) and CD3 and CD21 cells (E). (F) qPCR of indicated genes in WT and *Il27ra*$^{-/-}$ mouse synovium at d3 of AIA (n = 5–6/group). Error bars indicate SEM. *, P < 0.05; **, P < 0.01; ***, P < 0.001. Data are representative of two (A, C, D, E, and F) and four (B) independent experiments. Bars: (A and C) 200 µm; (D–E) 100 µm.

F4/80$^+$ myeloid cells were largely restricted to areas surrounding the lymphoid rich zones (Fig. 3 C), IHC detected the transcriptional regulator of Tfh cells and GC B cells, Bcl-6, and the fDC marker CD21 within their composition (Fig. 3, D and E). Thus, lymphoid aggregates in the inflamed synovium of *Il27ra*$^{-/-}$ mice resemble ELS.

To explore the initiation of ELS formation, we examined synovial expression of cytokines (*Il6*, *Il21*, *Ltb*, and *Vegf*), homeostatic chemokines (*Cxcl12*, *Cxcl13*, *Ccl19*, and *Ccl21*), and transcriptional regulators (*Bcl6* and *Prdm1*) linked with ectopic lymphoid neogenesis at d3 of AIA (Fig. 3 F; Manzo et al., 2005, 2010; Barone et al., 2008). Consistent with the presence of Bcl-6$^+$ lymphoid aggregates in *Il27ra*$^{-/-}$ mice, qPCR analysis showed increased synovial expression of *Bcl6* as compared with WT controls. No difference in *Il6*, *Il21*, *Ltb*, *Vegf*, *Cxcl12*, or *Prdm1* was seen between WT and *Il27ra*$^{-/-}$ mice (Fig. 3 F). Increased *Bcl6* expression was, however, accompanied by enhanced *Cxcl13* and *Ccl21* expression (Fig. 3 F), which steers the spatial organization of lymphoid cells within ELS (Luther et al., 2000; Chen et al., 2002). In contrast, synovial *Ccl19* expression was reduced in IL-27R deficiency. Although CCL19 and CCL21 share a common chemokine receptor (CCR7), they have a differential impact on composition and cellular organization of ELS (Luther et al., 2002; Haynes et al., 2007). Thus, relative differences in *Ccl19* and *Ccl21* expression within the inflamed synovium of *Il27ra*$^{-/-}$ mice may promote the CD3-rich nature of the observed ELS. By d10 of AIA, once ELSs were formed, expression of *Cxcl13* and *Ccl21* were comparable between WT and *Il27ra*$^{-/-}$ mice (Fig. 4 A). However, at this later time point, increased expression of the lymphoneogenic cytokines LTα and LTβ (*Lta* and *Ltb*) was observed in *Il27ra*$^{-/-}$ mice (Fig. 4 A). Similarly, synovial *Prdm1* (Blimp1) expression, which supports B cell differentiation into antibody-secreting plasma cells, was also heightened in *Il27ra*$^{-/-}$ mice at d10 (Fig. 4 A). These data are consistent with increased *Prdm1* expression in ectopic GCs after cytomegalovirus infection of salivary glands (Grewal et al., 2011). Thus,

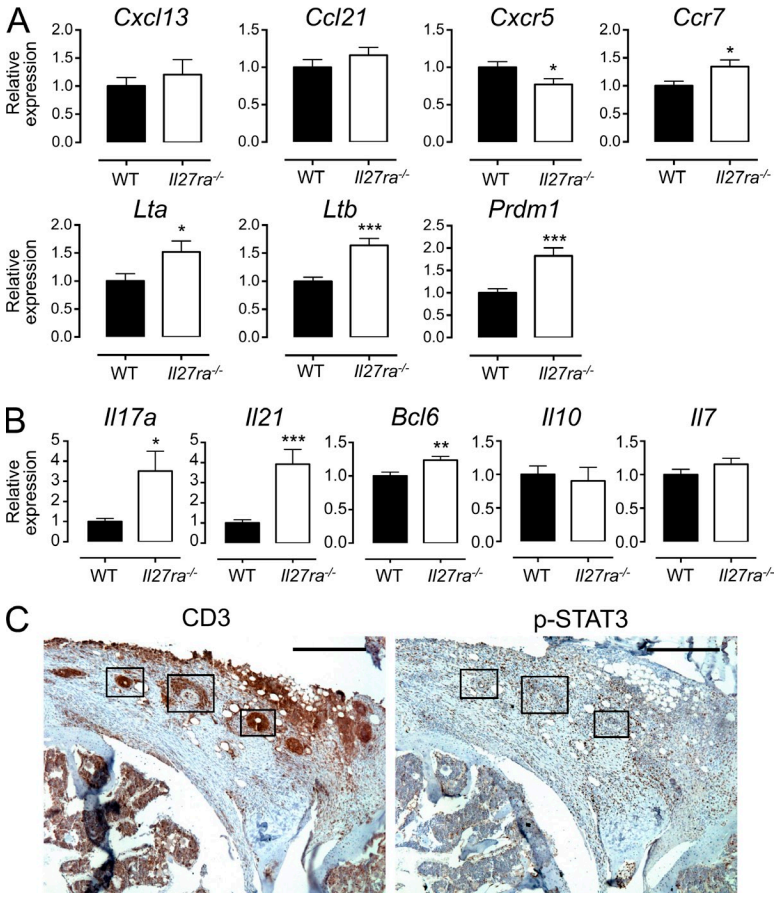

Figure 4. Synovial expression of ELS-associated signature genes in AIA. (A and B) qPCR of indicated genes in WT and *Il27ra*$^{-/-}$ mice at d10 of AIA (n = 15/group). Data are from three independent experiments. (C) Representative IHC of CD3 and phosphorylated (pY)-STAT3 synovial infiltrates in sequential sections at d10 of AIA in *Il27ra*$^{-/-}$ mice. Corresponding areas are boxed. Images are representative of four *Il27ra*$^{-/-}$ sections with ELS. Error bars indicate SEM. *, $P < 0.05$; **, $P < 0.01$; ***, $P < 0.001$. Bars, 200 µm.

IL-27 regulates synovial ELS through inhibition of homeostatic chemokines, lymphoid cytokines, and transcriptional regulators involved in lymphoid neogenesis.

IL-27 inhibits effector T cells linked with ELS formation

Recent studies have highlighted novel roles for effector T cell subsets, such as Th17 and Tfh cells, in ectopic lymphoid neogenesis and the control of GC reactions (Lu et al., 2011; Peters et al., 2011; Rangel-Moreno et al., 2011; Hirota et al., 2013). Thus, cytokines linked with either T cell differentiation or plasticity of effector T cells into Tfh-like phenotypes may regulate ELS involvement in chronic disease (Lu et al., 2011; Peters et al., 2011; Hirota et al., 2013). As IL-27 inhibits effector Th17 responses, we considered the expression of Th17 and Tfh cell markers within the inflamed synovium. At d10 of AIA, formation of ELS in *Il27ra*$^{-/-}$ mice was associated with increases in *Il17a* and the Tfh markers *Bcl6* and *Il21* (Fig. 4 B). No differences in *Il10* and *Il7* were observed between WT and *Il27ra*$^{-/-}$ mice.

The transcription factor STAT3 regulates Th17 and Tfh cell responses and is linked with lymphoid neogenesis and GC activities. In experimental arthritis, gp130-mediated STAT3 signaling exacerbates pathology (Atsumi et al., 2002; Nowell et al., 2009), and synovial tissues containing lymphoid follicles show enhanced STAT3 activity (Sawa et al., 2006; Timmer et al., 2007). IHC of infiltrating synovial leukocytes for tyrosine phosphorylated (pY)-STAT3 in *Il27ra*$^{-/-}$ mice revealed a high degree of STAT3 activity (Fig. 4 C). However, pY-STAT3 staining localized with diffuse infiltrates throughout the synovium and was not confined to ELS. Thus, localized STAT3 activity is an unreliable indicator of ELS and is consistent with the broader roles of STAT3 in governing chronic inflammation (Atsumi et al., 2002; Sawa et al., 2006; Nowell et al., 2009).

Recent studies have identified effector Th17 cells with Tfh-like properties that express the glycoprotein podoplanin (Pdp; gp38; Peters et al., 2011; Hirota et al., 2013). These cells contribute to ELS development in autoimmunity and GC reactions (Peters et al., 2011; Hirota et al., 2013; Miyamoto et al., 2013). Because *Il27ra*$^{-/-}$ mice show heightened peripheral Th17 responses (Fig. 2, E and F) and the local expression of Th17/Tfh markers during AIA (Figs. 3, D and E, and 4 B), we examined if synovial ELS development was linked to infiltrating Pdp-expressing T cells. Synovial tissue from AIA-challenged *Il27ra*$^{-/-}$ mice showed Pdp$^+$ cells colocalizing with B220$^+$ and CD3$^+$ cells at ELS (Fig. 5 A). Although Pdp$^+$ cells were enriched at ELS, staining was also seen in other areas (e.g., synovial lining). Indeed, synovial *Pdpn* expression remained comparable in WT and *Il27ra*$^{-/-}$ mice (Fig. 5 B). Whereas draining LNs from *Il27ra*$^{-/-}$ mice with AIA showed no increase in the total number of CD4$^+$Pdp$^+$ T cells (Fig. 5 C), an increased number of Pdp$^+$ Th17 cells were detected (Fig. 5 D).

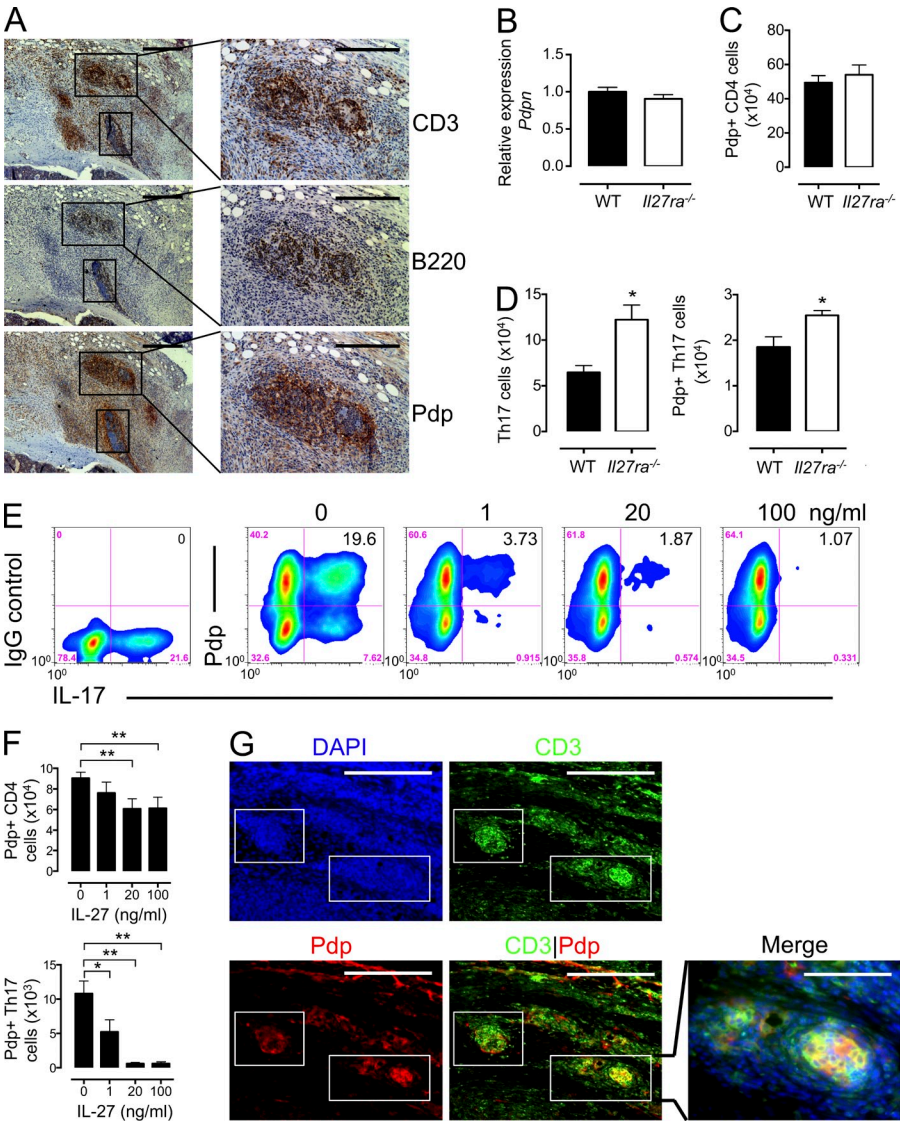

Figure 5. Pdp-expressing T helper cells are found at synovial ELS in *Il27ra*$^{-/-}$ mice. (A–D and G) AIA was established in WT and *Il27ra*$^{-/-}$ mice, and pathology was assessed at d10. (A) IHC of serial sections stained for CD3, B220, and Pdp in *Il27ra*$^{-/-}$ mice. ELS in sequential sections are shown boxed. Images are representative of four sections from two independent experiments. (B) qPCR of synovial *Pdpn* expression (n = 15/group from 3 independent experiments). (C and D) Number of Pdp$^+$ CD4 cells (C) and IL-17$^+$ and IL-17$^+$Pdp$^+$ Th17 cells (D) in inguinal LNs determined by flow cytometry (n = 8–9/group). Data are representative of two independent experiments. (E and F) WT CD4 T cells were activated under Th17-polarizing conditions with the indicated amount of IL-27 (0–100 ng/ml). Pdp$^+$ Th17 cell differentiation was determined by flow cytometry. Representative flow cytometry (E) and graphs (n = 3 mice) showing the number of CD4$^+$Pdp$^+$ T cells and CD4$^+$IL-17$^+$Pdp$^+$ T cells (Pdp$^+$ Th17 cells; F) after 4 d of culture. E and F are representative of three independent experiments. (G) Detection of Pdp$^+$ T cells at synovial ELS in *Il27ra*$^{-/-}$ mice by IF for Pdp and CD3 with DAPI nuclear staining. Images are representative of four sections from two independent experiments. Error bars indicate SEM. *, $P < 0.05$; **, $P < 0.01$. Bars: (A) 300 µm left, 200 µm right; (G, left) 200 µm left; (G, merged image) 100 µm.

To determine if IL-27 could suppress Pdp$^+$ Th17 cell development, naive CD4 T cells were cultured under Th17-polarizing conditions and expression of IL-17 and Pdp was assessed by flow cytometry (Fig. 5, E and F). Although IL-27 had a modest impact on the number of total CD4 cells expressing Pdp, IL-27 preferentially inhibited the expansion of Pdp$^+$IL-17$^+$ CD4 cells (Fig. 5, E and F). Subsequent IF studies of the inflamed synovium of *Il27ra*$^{-/-}$ mice revealed a colocalization of Pdp and CD3 in lymphoid aggregates (Fig. 5 G). Thus, synovial ELS in *Il27ra*$^{-/-}$ mice are associated with an increase in synovial Th17 and Tfh effector cytokines and peripheral Pdp$^+$ Th17 cell numbers. Therefore, IL-27 negatively regulates ELS development at sites of chronic inflammation through a potential impact on Th17 cells that can acquire Tfh-like properties.

IL-27 expression is decreased in lymphoid-rich synovitis

To translate our animal studies to clinical RA, expression of Th17/Tfh signatures were examined in synovial biopsies from ELS$^+$ and ELS$^-$ RA patients. In line with our mouse data, *IL17* and *IL21* were elevated in patients with ELS$^+$ synovitis, whereas no *IL17* transcripts were detected in patients with diffuse pathology (Fig. 6 A). *PDPN*, *BCL6*, and *IL10* expression was comparable in both patient groups. Consistent with data presented in Fig. 5 G, IF again confirmed the localization of Pdp in T cell–rich lymphoid aggregates in ELS$^+$ synovia (Fig. 6 B). Although Pdp expression was also seen in lymphatic compartments and synovial lining, it is perhaps significant that Pdp was only observed in ELS featuring full T/B cell segregation. Thus, Pdp detection in ELS may indicate functional GCs.

To link synovial histopathology with IL-27 involvement, expression of IL-27p28 (*IL27*) and Epstein-Barr virus-induced gene-3 (*EBI3*) were quantified in ELS$^+$ and ELS$^-$ RA patient biopsies and OA control tissue. Expression of *IL27* was significantly higher in ELS$^-$ RA patients compared with ELS$^+$ RA and OA biopsies (Fig. 6 C). Although *EBI3* showed a similar pattern of expression, the increase in ELS$^-$ tissue was not significant ($P = 0.8360$; Fig. 6 C). Detection of *IL27*

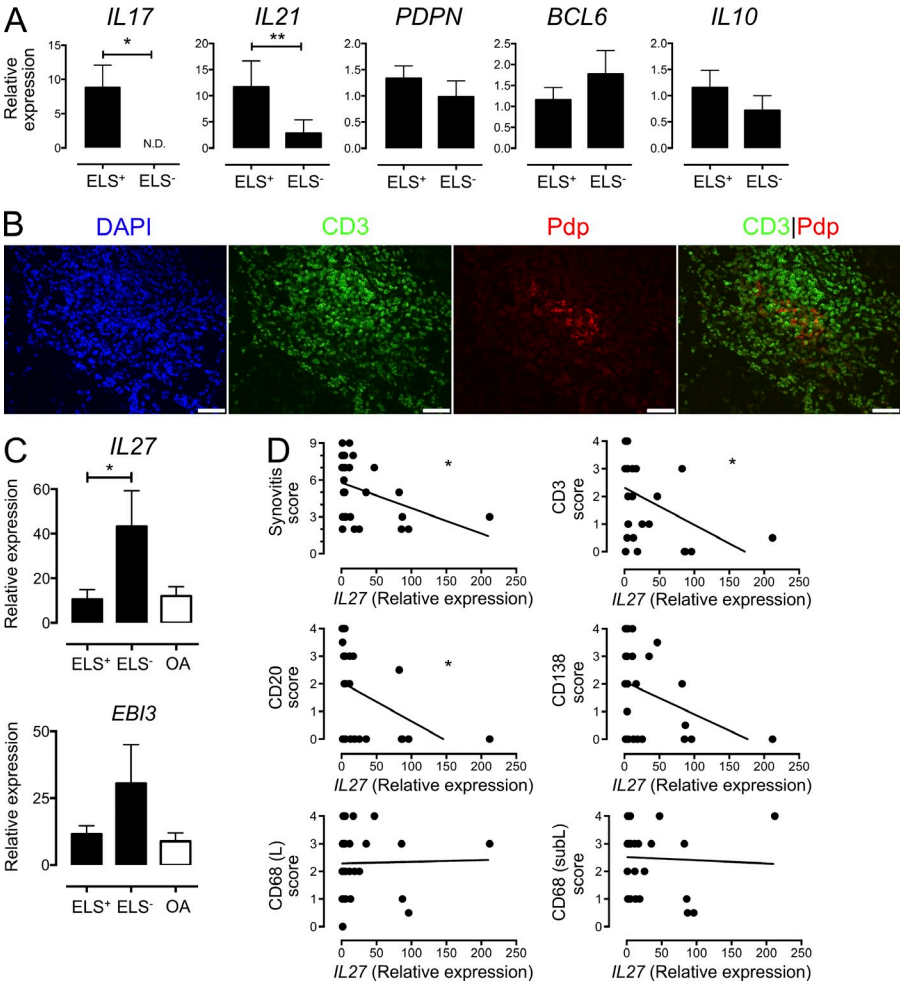

Figure 6. IL-27 expression reflects synovial histopathology in RA. (A) qPCR analysis of the indicated genes in synovia from ELS$^+$ and ELS$^-$ RA patients (*IL17*, $n = 23$ ELS$^+$, $n = 16$ ELS$^-$; *IL21*, $n = 28$ ELS$^+$, $n = 20$ ELS$^-$; *PDPN*, *BCL6*, and *IL10*, $n = 13$ ELS$^+$, $n = 12$ ELS$^-$). (B) Detection of Pdp$^+$ cells at synovial ELS by IF for Pdp and CD3 with DAPI nuclear staining. Images are representative of three tissue samples. (C) qPCR of *IL27* and *EBI3* expression in ELS$^+$ and ELS$^-$ RA synovia, and OA control patients ($n = 19$ ELS$^+$, $n = 14$ ELS$^-$, $n = 11$ OA). (D) Synovial *IL27* gene expression plotted against synovitis and IHC scores for CD3, CD20, CD138, and CD68 cells. Error bars indicate SEM; *, $P < 0.05$; **, $P < 0.01$. Bars, 50 µm.

inversely correlated with synovitis and CD3 and CD20 infiltration. However, no correlation was observed between *IL27* and IHC staining for CD138, or the myeloid marker CD68 (Fig. 6 D). Thus, *IL27* expression shows an inverse relationship to molecular signatures of ELS organization and function (Fig. 1 B). Synovial *IL27* expression is therefore predictive of patients with diffuse synovial histopathology and is consistent with the action of IL-27 as an inhibitor of ELS. Whereas the mechanism responsible for the pattern of *IL27* expression in different forms of synovitis is unclear, this likely reflects either inhibition of gene expression in ELS$^+$ patients or a specific induction in ELS$^-$ patients.

Early intervention is the most effective treatment for inflammatory arthritis. However, in the absence of reliable biomarkers, clinical criteria alone cannot predict the course of disease or the most suitable therapy for intervention. Defined patterns of synovial pathology emphasize the heterogeneity of RA progression and illustrate the importance of advances in biopsy techniques and diagnosis. Individuals with ELS$^+$ synovitis remain challenging to treat and typically respond poorly to anti-TNF (Cañete et al., 2009; Manzo et al., 2010). Our data shows that *IL27* is predictive of synovitis with diffuse inflammatory infiltrates, rather than highly organized ELSs. Although the mechanisms determining lymphoid-rich synovitis remains undefined, the ability to stratify patients with signature biomarkers such as *IL27* has the potential to inform treatment decisions by ensuring patients receive the most efficacious form of therapy for their type of disease.

MATERIALS AND METHODS

Clinical patient samples. Synovial tissue was collected from a total of 59 RA patients fulfilling the ACR criteria and undergoing arthroplastic surgery ($n = 23$) or ultrasound-guided synovial biopsy ($n = 36$) and 13 OA patients who underwent total joint replacement as control samples. Demographic data are provided in Table S1. The majority of patients had received stable-dose methotrexate, and none were on biologics. Paired paraffin-embedded tissue and RNA samples were prepared from all patients to allow cross-referencing between histological assessments and qPCR gene expression analysis. Procedures were approved by the hospital Ethics Committee (REC/98/11/27 Guys and St. Thomas' NHS Trust and REC 05/Q0703/198 Barts and The London NHS Trust) and performed after informed written consent.

For histological grading of tissues, 5-µm paraffin-embedded sections were stained with hematoxylin and eosin (H&E) to define the predominant histomorphological pattern of RA synovitis as either diffuse or aggregate. Synovial inflammation was graded as described previously (Humby et al., 2009), which is based on the enlargement of the synovial lining cell layer (score 0–3), the density of resident cells (0–3) and the extent of the inflammatory infiltrate (0–3) to yield a score ranging between 0 and 9. The degree of immune cell infiltration was further characterized by IHC using a

semi-quantitative analysis which grades (0–4) the degree of CD3 (T cells), CD20 (B cells), CD138 (plasma cells), and CD68 (macrophages) staining in the synovial and subsynovial lining (Fig. S1). To define the presence of ectopic lymphoid follicles, lymphoid aggregates were counted in each section and graded as described previously (Manzo et al., 2005; Humby et al., 2009), as grade 1 (G1) aggregates displaying a 2–5 radial cell number from a central blood vessel, grade 2 (G2), between 6–10 cells, or grade 3 (G3), with >10 cells. IHC staining for CD3, CD20, and CD21 was further used to confirm T/B cell segregation and the presence of follicular DC networks. Tissue with maximal G3 aggregates, staining positive for CD21 and displaying well-organized lymphoid structures, were defined as ELS^+. To minimize bias caused by anomalies in serial sectioning, all paraffin-embedded blocks were cut and stained at three levels 50 µm apart.

Animals. *Il27ra*$^{-/-}$ mice have been described previously (Yoshida et al., 2001). Mice were on a C57BL/6 background and were bred under specific pathogen–free conditions at Monash Institute of Medical Research (Clayton, Victoria, Australia) and Cardiff University (Cardiff, Wales). All experiments were endorsed by the Monash University Animal Ethics Committee and UK Home Office-approved project license PPL 30/2928.

Murine AIA. AIA was established in adult (8–12 wk) *Il27ra*$^{-/-}$ mice and age/sex-matched WT controls, as described previously (Nowell et al., 2009). In brief, mice were immunized by subcutaneous administration of 100 µl mBSA (1 mg/ml; Sigma-Aldrich) emulsified in an equal volume of Complete Freund's Adjuvant (CFA). To prime the immune response, mice also received 160 ng of heat-inactivated *Bordetella pertussis* toxin as a single intraperitoneal injection (Sigma-Aldrich). 1 wk later, mice were reimmunized with an identical subcutaneous administration of mBSA in CFA. 21 d after the initial immunization, inflammatory arthritis was triggered by intraarticular administration of 10 µl mBSA (10 mg/ml) in the right stifle joint. Animals were inspected daily for arthritis development by measuring knee joint diameters using a POCO 2T micrometer (Kroeplin). A minimum of six animals per time point was culled at intervals (days 3, 10, and 35) over the course of the disease, and joint pathology assessed histologically. Accumulative arthritic scores were generated according to the severity of synovial infiltration, exudate, hyperplasia, and joint erosion (see below).

Knee joints were fixed in neutral buffered formalin (10% vol/vol) and decalcified in 10% (vol/vol) formic acid at 4°C before embedding in paraffin. Midsagittal serial sections (7 µm thick) were stained with H&E. For evaluation of bone and cartilage erosion, sections were stained with Safranin O and Fast Green (Sigma-Aldrich). Two independent observers, blinded to the experimental groups, scored the sections for subsynovial inflammation (0 = normal to 5 = ablation of adipose tissue due to leukocyte infiltrate), synovial exudate (0 = normal to 3 = substantial number of cells with large fibrin deposits), synovial hyperplasia (0 = normal 1–3 cells thick to 3 = over 3 layers thick with overgrowth onto joint surfaces with evidence of cartilage/bone erosion), and cartilage/bone erosion (0 = normal to 3 = destruction of a significant part of the bone). The aggregate score for all parameters is presented as an arthritic index.

Quantitative real-time PCR. For mouse samples, the inflamed synovium was recovered by dissection before storing in RNA*later* (Ambion) at −80°C. Total cellular RNA was extracted using TRIsure reagent (Bioline) and further purified using the RNeasy Mini kit with on-column DNase treatment (QIAGEN). RNA was converted to cDNA using the nanoScript 2 Reverse Transcription kit (Primerdesign). Expression of mouse genes was determined using the 7900HT Fast or the QuantStudio 12K Flex Real-Time PCR System, and data acquisition and analyses were performed using the Sequences Detection System Version 2.3 software and ExpressionSuite software version 1.0.3 (all from Life Technologies). Sequences of primers used with SYBR Green reagents (Invitrogen) can be seen in Table S2. All other genes were analyzed using TaqMan primers, probes, and reaction buffers (Life Technologies). Genes were normalized against the expression of the housekeeping genes for 18S rRNA and ACTB.

Clinical patient synovial samples were stored in RNA*later* at −80°C. RNA was recovered as above using the RNeasy Mini kit (QIAGEN) and cDNA prepared using the Thermoscript RT-PCR System for Fist-Strand cDNA Synthesis kit (Invitrogen). Gene expression was quantified using TaqMan primers, probes, and reaction buffers and acquired on a 7900HT Fast Real Time PCR System (all Life Technologies). Genes were normalized against the expression of the housekeeping genes for 18S rRNA and GAPDH.

Immunohistochemistry. Leukocyte and follicular markers were detected in paraffin sections using primary antibodies to murine CD3 (Dako), F4/80 (AbD Serotec), B220 (BD), CD21, and Bcl-6 (Santa Cruz Biotechnology, Inc.) and podoplanin (BioLegend). Antigen unmasking was achieved by heating in 10 mM sodium citrate buffer containing 0.05% (wt/vol) Tween 20 (95°C, 40 min). For F4/80 staining, antigen retrieval was performed by incubating with 0.05% (wt/vol) Trypsin-EDTA (37°C, 30 min). Endogenous peroxidase and biotin activity was blocked using 3% (vol/vol) H_2O_2 and an avidin/biotin blocking kit (Vector Laboratories), respectively. Sections were incubated in serum appropriate to the secondary antibody before primary antibody incubations. Antibody labeling was detected using biotinylated secondary antibodies (Dako), the Vectastain ABC kit and diaminobenzidine chromagen (Vector Laboratories). Sections were counterstained with hematoxylin. The Leica QWin microscope imaging software was used for quantification of staining. Colocalization of lymphoid cells was determined by staining of serial, sequential sections.

Immunofluorescence. Paraffin-embedded sections were rehydrated before antigen unmasking by incubating in target retrieval solution (Dako) at 95°C for 35 min for human synovium or 10 mM sodium citrate buffer containing 0.05% (wt/vol) Tween 20 (95°C, 40 min) for mouse. Endogenous biotin activity was blocked using the avidin/biotin blocking kit (Vector Laboratories). Human synovial sections were incubated with serum-free protein block (Dako) before incubation with goat anti–human IL-27R (R&D Systems), mouse anti–human podoplanin, or mouse anti–human CD3 (both Dako). Mouse sections were blocked with goat serum before incubation with antibodies to podoplanin (BioLegend) or CD3 (Dako). Antibody labeling was detected using combinations of biotinylated and Alexa Fluor 488–conjugated secondary antibodies, and Alexa Fluor 555 or APC-conjugated streptavidin. Slides were counter stained with DAPI and mounted with Mowiol.

In vitro T cell cultures. Naive CD4 T cells ($CD4^+CD25^-CD44^{lo}CD62L^{hi}$) cells were cultured in RPMI-1640 supplemented with 10% (vol/vol) FCS, 2 mM L-glutamine, 100 U/ml penicillin, 100 µg/ml streptomycin, 1 mM sodium pyruvate, and 50 µM 2-mercaptoethanol (all from Invitrogen). 10^5 cells were cultured in 96-well plates coated with anti-CD3 (1 µg/ml; 145-2C11) and soluble anti-CD28 (5 µg/ml; 37.51). Cultures contained recombinant TGFβ (1 ng/ml) and IL-6 (20 ng/ml) with or without IL-27 (1–100 ng/ml) as indicated.

Flow cytometry. Inguinal LNs were recovered and single-cell suspensions prepared and analyzed by flow cytometry. For intracellular cytokine staining, cells were cultured with PMA (50 ng/ml), ionomycin (500 ng/ml), and monensin (3 µM; all from Sigma-Aldrich) for 4 h. Cells were stained for cell surface markers, then fixed and permeabilized in Cytofix/Cytoperm (BD) before intracellular detection of cytokines. Flow cytometric analysis of cells was performed using anti-CD4 (RM4-5), anti-CD3 (17A2), anti-IL-17 (TC11-18H10.1), anti-IFN-γ (XMG1.2), and anti-podoplanin (8.1.1). Cells were acquired using a FACSCanto II (BD) or CyAn ADP (Beckman Coulter) flow cytometer and analyzed using FlowJo software (Tree Star). Cell numbers were determined by multiplying the percentage obtained by flow cytometry with the total cell count.

Enzyme-linked immunosorbent assay (ELISA). IL-17A levels were determined in mouse serum using a commercial murine IL-17A ELISA kit (BioLegend). Serum antibody titers to mBSA were determined by coating

microtiter plates with mBSA diluted in PBS (5 µg/ml). Nonspecific binding sites were blocked with 5% (wt/vol) milk extract in PBS containing 0.05% (wt/vol) Tween-20. Sera were diluted 1/1,000 in PBS containing milk extract and Tween-20 before adding to the microplates for 2 h. Antibody levels were detected using HRP-conjugated anti–mouse IgG and tetramethylbenzidine substrate. Absorbance was measured at 450 nm.

Statistics. Statistical analysis was performed using GraphPad Prism software. For assessment of arthritic indices, significant differences were determined using the nonparametric Mann Whitney *U* test. Otherwise, statistical differences were determined using the unpaired Student's *t* test. Where experimental groups were compared across multiple time points, a two-way analysis of variance (ANOVA) was used with the Bonferroni post-test. For clinical samples, data displaying nonnormal distribution was analyzed using the nonparametric Mann Whitney *U* test. Normally distributed data were analyzed using the Student's *t* test. $P < 0.05$ was considered significant. Graphs represent mean ± SEM.

Online supplemental material. Fig. S1 shows a histopathology reference atlas for scoring RA synovial tissue. Table S1 shows the clinical characteristics of the RA and OA patients. Table S2 lists primer sequences used in this study for SYBR Green-based qPCR. Online supplemental material is available at http://www.jem.org/cgi/content/full/jem.20132307/DC1.

This work was supported by an Arthritis Research UK grant funding (20770, 20305, 19796, 19381, 18286 to G.W. Jones, A.S. Williams, and S.A. Jones), the Wellcome Trust ISSF Seedcorn and Mobility Awards (to G.W. Jones and S.A. Jones), the National Health and Medical Research Council (NHMRC, Australia; to B.J. Jenkins), as well as the Operational Infrastructure Support Program by the Victorian Government of Australia. B.J. Jenkins is recipient of Senior Medical Research Fellowships awarded by the Sylvia and Charles Viertel Foundation (2009–2013) and NHMRC (2014–present).

The authors declare no competing financial interests.

Authors contributions: G.W. Jones, S.A. Jones, and B.J. Jenkins designed the study and performed the experiments. C.J. Greenhill, L. McLeod, and A.S. Williams contributed to the analysis of experimental arthritis samples. A. Cardus contributed to analysis of in vitro experiments. M. Bombardieri, V. Rocher-Ros, A. Nerviani, and C. Pitzalis contributed clinical specimens, histopathological characterization, and analysis of clinical samples. G.W. Jones, S.A. Jones, and B.J. Jenkins wrote the paper.

Submitted: 4 November 2013
Accepted: 28 August 2015

REFERENCES

Atsumi, T., K. Ishihara, D. Kamimura, H. Ikushima, T. Ohtani, S. Hirota, H. Kobayashi, S.J. Park, Y. Saeki, Y. Kitamura, and T. Hirano. 2002. A point mutation of Tyr-759 in interleukin 6 family cytokine receptor subunit gp130 causes autoimmune arthritis. *J. Exp. Med.* 196:979–990. http://dx.doi.org/10.1084/jem.20020619

Avouac, J., L. Gossec, and M. Dougados. 2006. Diagnostic and predictive value of anti-cyclic citrullinated protein antibodies in rheumatoid arthritis: a systematic literature review. *Ann. Rheum. Dis.* 65:845–851. http://dx.doi.org/10.1136/ard.2006.051391

Barone, F., M. Bombardieri, M.M. Rosado, P.R. Morgan, S.J. Challacombe, S. De Vita, R. Carsetti, J. Spencer, G. Valesini, and C. Pitzalis. 2008. CXCL13, CCL21, and CXCL12 expression in salivary glands of patients with Sjogren's syndrome and MALT lymphoma: association with reactive and malignant areas of lymphoid organization. *J. Immunol.* 180: 5130–5140. http://dx.doi.org/10.4049/jimmunol.180.7.5130

Cañete, J.D., R. Celis, C. Moll, E. Izquierdo, S. Marsal, R. Sanmartí, A. Palacín, D. Lora, J. de la Cruz, and J.L. Pablos. 2009. Clinical significance of synovial lymphoid neogenesis and its reversal after anti-tumour necrosis factor alpha therapy in rheumatoid arthritis. *Ann. Rheum. Dis.* 68:751–756. http://dx.doi.org/10.1136/ard.2008.089284

Chen, S.C., G. Vassileva, D. Kinsley, S. Holzmann, D. Manfra, M.T. Wiekowski, N. Romani, and S.A. Lira. 2002. Ectopic expression of the murine chemokines CCL21a and CCL21b induces the formation of lymph node-like structures in pancreas, but not skin, of transgenic mice. *J. Immunol.* 168:1001–1008. http://dx.doi.org/10.4049/jimmunol.168.3.1001

Grewal, J.S., M.J. Pilgrim, S. Grewal, L. Kasman, P. Werner, M.E. Bruorton, S.D. London, and L. London. 2011. Salivary glands act as mucosal inductive sites via the formation of ectopic germinal centers after site-restricted MCMV infection. *FASEB J.* 25:1680–1696. http://dx.doi.org/10.1096/fj.10-174656

Haynes, N.M., C.D. Allen, R. Lesley, K.M. Ansel, N. Killeen, and J.G. Cyster. 2007. Role of CXCR5 and CCR7 in follicular Th cell positioning and appearance of a programmed cell death gene-1high germinal center-associated subpopulation. *J. Immunol.* 179:5099–5108. http://dx.doi.org/10.4049/jimmunol.179.8.5099

Hirota, K., J.E. Turner, M. Villa, J.H. Duarte, J. Demengeot, O.M. Steinmetz, and B. Stockinger. 2013. Plasticity of Th17 cells in Peyer's patches is responsible for the induction of T cell-dependent IgA responses. *Nat. Immunol.* 14:372–379. http://dx.doi.org/10.1038/ni.2552

Humby, F., M. Bombardieri, A. Manzo, S. Kelly, M.C. Blades, B. Kirkham, J. Spencer, and C. Pitzalis. 2009. Ectopic lymphoid structures support ongoing production of class-switched autoantibodies in rheumatoid synovium. *PLoS Med.* 6:e1. http://dx.doi.org/10.1371/journal.pmed.0060001

Kalliolias, G.D., B. Zhao, A. Triantafyllopoulou, K.H. Park-Min, and L.B. Ivashkiv. 2010. Interleukin-27 inhibits human osteoclastogenesis by abrogating RANKL-mediated induction of nuclear factor of activated T cells c1 and suppressing proximal RANK signaling. *Arthritis Rheum.* 62:402–413. http://dx.doi.org/10.1002/art.27200

Klimiuk, P.A., J.J. Goronzy, J. Björ nsson, R.D. Beckenbaugh, and C.M. Weyand. 1997. Tissue cytokine patterns distinguish variants of rheumatoid synovitis. *Am. J. Pathol.* 151:1311–1319.

Lu, K.T., Y. Kanno, J.L. Cannons, R. Handon, P. Bible, A.G. Elkahloun, S.M. Anderson, L. Wei, H. Sun, J.J. O'Shea, and P.L. Schwartzberg. 2011. Functional and epigenetic studies reveal multistep differentiation and plasticity of in vitro-generated and in vivo-derived follicular T helper cells. *Immunity.* 35:622–632. http://dx.doi.org/10.1016/j.immuni.2011.07.015

Luther, S.A., T. Lopez, W. Bai, D. Hanahan, and J.G. Cyster. 2000. BLC expression in pancreatic islets causes B cell recruitment and lymphotoxin-dependent lymphoid neogenesis. *Immunity.* 12:471–481. http://dx.doi.org/10.1016/S1074-7613(00)80199-5

Luther, S.A., A. Bidgol, D.C. Hargreaves, A. Schmidt, Y. Xu, J. Paniyadi, M. Matloubian, and J.G. Cyster. 2002. Differing activities of homeostatic chemokines CCL19, CCL21, and CXCL12 in lymphocyte and dendritic cell recruitment and lymphoid neogenesis. *J. Immunol.* 169: 424–433. http://dx.doi.org/10.4049/jimmunol.169.1.424

Manzo, A., S. Paoletti, M. Carulli, M.C. Blades, F. Barone, G. Yanni, O. Fitzgerald, B. Bresnihan, R. Caporali, C. Montecucco, et al. 2005. Systematic microanatomical analysis of CXCL13 and CCL21 in situ production and progressive lymphoid organization in rheumatoid synovitis. *Eur. J. Immunol.* 35:1347–1359. http://dx.doi.org/10.1002/eji.200425830

Manzo, A., M. Bombardieri, F. Humby, and C. Pitzalis. 2010. Secondary and ectopic lymphoid tissue responses in rheumatoid arthritis: from inflammation to autoimmunity and tissue damage/remodeling. *Immunol. Rev.* 233:267–285. http://dx.doi.org/10.1111/j.0105-2896.2009.00861.x

Miyamoto, Y., H. Uga, S. Tanaka, M. Kadowaki, M. Ikeda, J. Saegusa, A. Morinobu, S. Kumagai, and H. Kurata. 2013. Podoplanin is an inflammatory protein upregulated in Th17 cells in SKG arthritic joints. *Mol. Immunol.* 54:199–207. http://dx.doi.org/10.1016/j.molimm.2012.11.013

Niedbala, W., B. Cai, X. Wei, A. Patakas, B.P. Leung, I.B. McInnes, and F.Y. Liew. 2008. Interleukin 27 attenuates collagen-induced arthritis. *Ann. Rheum. Dis.* 67:1474–1479. http://dx.doi.org/10.1136/ard.2007.083360

Nowell, M.A., A.S. Williams, S.A. Carty, J. Scheller, A.J. Hayes, G.W. Jones, P.J. Richards, S. Slinn, M. Ernst, B.J. Jenkins, et al. 2009. Therapeutic targeting of IL-6 trans signaling counteracts STAT3 control of experimental inflammatory arthritis. *J. Immunol.* 182:613–622. http://dx.doi.org/10.4049/jimmunol.182.1.613

Owaki, T., M. Asakawa, S. Kamiya, K. Takeda, F. Fukai, J. Mizuguchi, and T. Yoshimoto. 2006. IL-27 suppresses CD28-mediated [correction of medicated] IL-2 production through suppressor of cytokine signaling 3. *J. Immunol.* 176:2773–2780. http://dx.doi.org/10.4049/jimmunol.176.5.2773

Peters, A., L.A. Pitcher, J.M. Sullivan, M. Mitsdoerffer, S.E. Acton, B. Franz, K. Wucherpfennig, S. Turley, M.C. Carroll, R.A. Sobel, et al. 2011. Th17 cells induce ectopic lymphoid follicles in central nervous system tissue inflammation. *Immunity*. 35:986–996. http://dx.doi.org/10.1016/j.immuni.2011.10.015

Pickens, S.R., N.D. Chamberlain, M.V. Volin, A.M. Mandelin II, H. Agrawal, M. Matsui, T. Yoshimoto, and S. Shahrara. 2011. Local expression of interleukin-27 ameliorates collagen-induced arthritis. *Arthritis Rheum.* 63:2289–2298. http://dx.doi.org/10.1002/art.30324

Pitzalis, C., S. Kelly, and F. Humby. 2013. New learnings on the pathophysiology of RA from synovial biopsies. *Curr. Opin. Rheumatol.* 25:334–344. http://dx.doi.org/10.1097/BOR.0b013e32835fd8eb

Rangel-Moreno, J., D.M. Carragher, M. de la Luz Garcia-Hernandez, J.Y. Hwang, K. Kusser, L. Hartson, J.K. Kolls, S.A. Khader, and T.D. Randall. 2011. The development of inducible bronchus-associated lymphoid tissue depends on IL-17. *Nat. Immunol.* 12:639–646. http://dx.doi.org/10.1038/ni.2053

Rosengren, S., N. Wei, K.C. Kalunian, N.J. Zvaifler, A. Kavanaugh, and D.L. Boyle. 2008. Elevated autoantibody content in rheumatoid arthritis synovia with lymphoid aggregates and the effect of rituximab. *Arthritis Res. Ther.* 10:R105. http://dx.doi.org/10.1186/ar2497

Sawa, S., D. Kamimura, G.H. Jin, H. Morikawa, H. Kamon, M. Nishihara, K. Ishihara, M. Murakami, and T. Hirano. 2006. Autoimmune arthritis associated with mutated interleukin (IL)-6 receptor gp130 is driven by STAT3/IL-7–dependent homeostatic proliferation of $CD4^+$ T cells. *J. Exp. Med.* 203:1459–1470. http://dx.doi.org/10.1084/jem.20052187

Stumhofer, J.S., A. Laurence, E.H. Wilson, E. Huang, C.M. Tato, L.M. Johnson, A.V. Villarino, Q. Huang, A. Yoshimura, D. Sehy, et al. 2006. Interleukin 27 negatively regulates the development of interleukin 17-producing T helper cells during chronic inflammation of the central nervous system. *Nat. Immunol.* 7:937–945. http://dx.doi.org/10.1038/ni1376

Takemura, S., A. Braun, C. Crowson, P.J. Kurtin, R.H. Cofield, W.M. O'Fallon, J.J. Goronzy, and C.M. Weyand. 2001. Lymphoid neogenesis in rheumatoid synovitis. *J. Immunol.* 167:1072–1080. http://dx.doi.org/10.4049/jimmunol.167.2.1072

Tanida, S., H. Yoshitomi, M. Ishikawa, T. Kasahara, K. Murata, H. Shibuya, H. Ito, and T. Nakamura. 2011. IL-27-producing CD14(+) cells infiltrate inflamed joints of rheumatoid arthritis and regulate inflammation and chemotactic migration. *Cytokine*. 55:237–244. http://dx.doi.org/10.1016/j.cyto.2011.04.020

Timmer, T.C., B. Baltus, M. Vondenhoff, T.W. Huizinga, P.P. Tak, C.L. Verweij, R.E. Mebius, and T.C. van der Pouw Kraan. 2007. Inflammation and ectopic lymphoid structures in rheumatoid arthritis synovial tissues dissected by genomics technology: identification of the interleukin-7 signaling pathway in tissues with lymphoid neogenesis. *Arthritis Rheum.* 56:2492–2502. http://dx.doi.org/10.1002/art.22748

Villarino, A., L. Hibbert, L. Lieberman, E. Wilson, T. Mak, H. Yoshida, R.A. Kastelein, C. Saris, and C.A. Hunter. 2003. The IL-27R (WSX-1) is required to suppress T cell hyperactivity during infection. *Immunity*. 19:645–655. http://dx.doi.org/10.1016/S1074-7613(03)00300-5

Wong, C.K., P. Chen, L.S. Tam, E.K. Li, Y.B. Yin, and C.W. Lam. 2010. Effects of inflammatory cytokine IL-27 on the activation of fibroblast-like synoviocytes in rheumatoid arthritis. *Arthritis Res. Ther.* 12:R129. http://dx.doi.org/10.1186/ar3067

Yoshida, H., S. Hamano, G. Senaldi, T. Covey, R. Faggioni, S. Mu, M. Xia, A.C. Wakeham, H. Nishina, J. Potter, et al. 2001. WSX-1 is required for the initiation of Th1 responses and resistance to *L. major* infection. *Immunity*. 15:569–578. http://dx.doi.org/10.1016/S1074-7613(01)00206-0